A Phase II Study of 3′-Deoxy-3′-18F-Fluorothymidine PET in the Assessment of Early Response of Breast Cancer to Neoadjuvant Chemotherapy: Results from ACRIN 6688

Lale Kostakoglu[1], **Fenghai Duan**[2], **Michael O. Idowu**[3], **Paul R. Jolles**[3], **Harry D. Bear**[3,4], **Mark Muzi**[5], **Jean Cormack**[2], **John P. Muzi**[5], **Daniel A. Pryma**[6], **Jennifer M. Specht**[5], **Linda Hovanessian-Larsen**[7], **John Miliziano**[8], **Sharon Mallett**[9], **Anthony F. Shields**[10], and **David A. Mankoff**[6] **on behalf of the ACRIN 668 Investigative Team**

[1]Department of Radiology, Icahn School of Medicine at Mount Sinai, New York, New York
[2]Department of Biostatistics and Center for Statistical Sciences, Brown University School of Public Health, Providence, Rhode Island [3]Virginia Commonwealth University, Richmond, Virginia [4]Massey Cancer Center of Virginia Commonwealth University, Richmond, Virginia [5]University of Washington, Seattle, Washington [6]Abramson Cancer Center and Perelman School of Medicine University of Pennsylvania, Philadelphia, Pennsylvania [7]University of Southern California, Los Angeles, California [8]Morton Mease Plant Hospital, Clearwater, Florida [9]American College of Radiology Imaging Network (ACRIN), Philadelphia, Pennsylvania [10]Karmanos Cancer Institute, Wayne State University, Detroit, Michigan

Abstract

Our objective was to determine whether early change in standardized uptake values (SUVs) of 3′deoxy-3′-18F-fluorothymidine (18F-FLT) using PET with CT could predict pathologic complete response (pCR) of primary breast cancer to neoadjuvant chemotherapy (NAC). The key secondary objective was to correlate SUV with the proliferation marker Ki-67 at baseline and after NAC.

Methods—This prospective, multicenter phase II study did not specify the therapeutic regimen, thus, NAC varied among centers. All evaluable patients underwent 18F-FLT PET/CT at baseline (FLT1) and after 1 cycle of NAC (FLT2); 43 patients were imaged at FLT1, FLT2, and after NAC completion (FLT3). The percentage change in maximum SUV (% SUV_{max}) between FLT1 and FLT2 and FLT3 was calculated for the primary tumors. The predictive value of SUV_{max} for pCR was determined using receiver-operating-characteristic curve analysis. The correlation between SUV_{max} and Ki-67 was also assessed.

Results—Fifty-one of 90 recruited patients (median age, 54 y; stage IIA–IIIC) met the eligibility criteria for the primary objective analysis, with an additional 22 patients totaling 73 patients for secondary analyses. A pCR in the primary breast cancer was achieved in 9 of 51 patients. NAC

For correspondence or reprints contact: Lale Kostakoglu, Icahn School of Medicine at Mount Sinai, Mount Sinai Medical Center, Department of Radiology, Division of Nuclear Medicine, One Gustave L. Levy Place, P.O. Box 1141, New York, NY 10029.

resulted in a significant reduction in %SUV_{max} (mean , 39%; 95% confidence interval, 31–46). There was a marginal difference in % $SUV_{max\_FLT1-FLT2}$ between pCR and no-pCR patient groups (Wilcoxon 1-sided $P = 0.050$). The area under the curve for SUV_{max} in the prediction of pCR was 0.68 (90% confidence interval, 0.50–0.83; Delong 1-sided $P = 0.05$), with slightly better predictive value for percentage mean SUV ($P = 0.02$) and similar prediction for peak SUV ($P = 0.04$). There was a weak correlation with pretherapy SUV_{max} and Ki-67 ($r = 0.29$, $P = 0.04$), but the correlation between SUV_{max} and Ki-67 after completion of NAC was stronger ($r = 0.68$, $P < 0.0001$).

Conclusion—[18]F-FLT PET imaging of breast cancer after 1 cycle of NAC weakly predicted pCR in the setting of variable NAC regimens. Posttherapy ^{18}F-FLT uptake correlated with Ki-67 on surgical specimens. These results suggest some efficacy of ^{18}F-FLT as an indicator of early therapeutic response of breast cancer to NAC and support future multicenter studies to test ^{18}F-FLT PET in a more uniformly treated patient population.

Keywords

early treatment response; ^{18}F-FLT PET; breast cancer; neoadjuvant therapy

Systemic neoadjuvant chemotherapy (NAC) before surgery plays a role in locally advanced breast cancer to downstage disease to increase the chances for breast-conserving surgery, eradicate micro-metastases, and provide an indication of therapeutic responsiveness (1). The eradication of invasive cancer after NAC, that is, pathologic complete response (pCR), is a predictor of improved survival (2,3). However, conventional chemotherapy regimens result in pCR in only a minority of patients. In the era of individualized medicine, assessing pathologic response after completion of NAC does not allow for therapy adaptation with earlier discontinuation of ineffective therapies. Patients without sufficient response might benefit from switching to more effective alternative treatments early during the course of NAC. In this regard, there is a need to develop noninvasive imaging methodologies that can provide an early indication of response. Currently, treatment response is largely assessed by measurement of tumor size after several cycles of chemotherapy. Size changes can lag behind therapy-induced molecular changes, motivating the use of molecular imaging methods to assess response. Although ^{18}F-FDG PET has been used commonly to monitor response to treatment in breast cancer, it has limitations that include prediction of pCR across different phenotypes (4,5). PET imaging with 3′-deoxy-3′-^{18}F-fluorothymidine (^{18}F-FLT) PET provides a noninvasive method for evaluating cell proliferation, an early indicator of therapeutic response. ^{18}F-FLT is a substrate for thymidine kinase-1, and the accumulation of ^{18}F-FLT in tumors provides a quantitative measure of cell proliferation through the relationship between thymidine kinase-1 expression and cell cycle regulation (6–9). Several prior single-center studies have demonstrated that changes in breast cancer tumor proliferation assessed by ^{18}F-FLT PET/CT early after initiating chemotherapy predict tumor response with good sensitivity; however, the results of these studies were variable and none of the prior studies investigated the potential for predicting pCR to NAC (10–17). In the present multicenter study, our objective was to correlate changes measured by ^{18}F-FLT in the primary tumor early during NAC with pCR in locally advanced breast cancer patients. We also studied both pretherapy and post-therapy association of ^{18}F-FLT uptake with the

tissue proliferative marker Ki-67 to compare ^{18}F-FLT PET/CT against an accepted reference standard for cellular proliferation.

MATERIALS AND METHODS

Patients and Study Design

American College of Radiology Imaging Network (ACRIN) 6688 was an observational, nonrandomized, multicenter phase II study. This study was approved by the Institutional Review Board of each participating center, and all subjects signed a written informed consent form. The primary objective was to correlate the percentage change in maximum standardized uptake value (SUV_{max}) between pretherapy (FLT1) and ^{18}F-FLT PET/CT after 1 cycle (FLT2) (% $SUV_{max\_FLT1-FLT2}$) of NAC with pCR in breast cancer patients for whom NAC was clinically indicated. The eligibility criteria included histologically confirmed breast cancer diagnosis, primary breast cancer measuring greater than or equal to 2.0 cm, being a candidate for NAC and surgical resection of residual primary tumor after NAC, and no evidence of stage IV disease. The chemotherapy regimens chosen for each patient were not specified by trial design as long as the patients were on a treatment containing cytotoxic agents as key components of the regimen. Hormonal and other targeted therapies were allowed, but only when given in association with chemotherapy agents. The eligible patients were planned to undergo 3 ^{18}F-FLT PET/CT studies, FLT1, FLT2, and after completion of NAC before surgery (FLT3).

The key secondary objectives were to measure the correlation between FLT1 and FLT3 uptake parameters and immunohistochemical (Ki-67) analysis of pretherapy biopsy and posttherapy surgical specimens, respectively. Other secondary objectives included in this report were to evaluate the relationship between FLT1, FLT2, and FLT3 uptake parameters and pCR of the primary tumor and residual cancer burden (RCB) (18) and pCR to NAC in lymph node (LN) metastases, as well as to confirm safety and define adverse effects of ^{18}F-FLT.

^{18}F-FLT PET/CT Protocol

^{18}F-FLT was used under the authority of a National Cancer Institute–sponsored investigational new drug application. After the injection of 2.6 MBq/kg (mean, 167 MBq; range, 110–204 MBq), a whole-body image (5–7 bed positions) was obtained at 60 min (mean, 70 min; range, 50–101 min). All patients were scanned on calibrated and ACRIN-accredited PET/CT scanners, which included review of image quality and testing of SUVs using a uniform phantom and review of images as previously reported (19). A static torso survey was acquired for all patients. Sixty-minute dynamic regional PET/CT imaging was optional (results not included in this report). When used, dynamic PET imaging was performed first, followed by the torso survey using static PET imaging. There were 3 planned ^{18}F-FLT PET/CT sessions. Baseline (FLT1) scanning was completed within 4 wk before NAC initiation. The early therapy (FLT2) scan was planned at 5–10 d after the initiation of the first cycle of the NAC and before the second cycle of NAC. Posttherapy ^{18}F-FLT (FLT3) was performed after the completion of NAC and within 3 wk before surgery. All sequential imaging sessions were performed on identical or technically

equivalent PET/CT scanners for any individual patient. An adverse event evaluation was performed at each imaging time point. After completion of NAC, the subjects underwent surgical resection of the breast primary (segmental or total mastectomy) and axillary nodal evaluation.

^{18}F-FLT PET/CT Image Data Analysis

All ^{18}F-FLT PET/CT images were transferred to the ACRIN Core Laboratory for quality control, archiving, and analysis. Primary image interpretation was based on semiquantitative analysis (SUV) at a Core Laboratory site at the University of Washington. Image review and region placement was supervised by 2 nuclear medicine board-certified physicians with extensive experience in PET/CT, masked to patient characteristics and outcome. Participating sites first indicated up to 3 primary tumor locations and up to 5 other nonprimary tumors based on local interpretation. At the Core Laboratory, volumes of interest (VOIs) were positioned over the area of highest activity for both the primary and the nonprimary breast tumors at FLT1. The SUV_{peak}, defined as the average SUV from a 1.0-cm-diameter circular VOI (range of 0.75–1.5 cm, depending on scanner resolution) centered over the hottest tumor pixel at FLT1, was also created. VOIs were constructed on FLT2 and FLT3 images based on CT localization, and residual tumor uptake when present, for all sites visualized at FLT1. The VOIs for FLT1, FLT2, FLT3 were verified independently by 2 expert reviewers masked to the clinical and pathologic results. The SUV_{peak}, as described above; the SUV_{mean}, the average SUV tumor value; and SUV_{max}, the maximal pixel intensity in the 1-mL tumor VOI, were recorded. For multiple primary tumors, the mean SUV_{max} for all tumor sites was used as the patient's overall tumor SUV. The axillary LNs were analyzed using the same methodology, including only those LNs measuring 1.0 cm or greater in maximum dimension on CT to minimize partial-volume effects. No partial-volume corrections of the SUVs were attempted given the challenges of determining tumor boundaries from CT and the variability of the included scanner types.

Histopathology Analysis

The paraffin blocks or 5 unstained sections containing tumor tissue from the diagnostic biopsy and posttreatment surgical specimen were collected and sent to the Core Pathology Laboratory at Virginia Commonwealth University (CPL-VCU) for analysis. No additional biopsy was obtained. If there was residual tumor on posttreatment specimens, a representative section was acceptable but if no residual tumor was present per original pathology reports or in the posttreatment section, the entire tumor bed was sectioned to confirm pCR. If no viable or residual tumor remained on review of all sections, a pCR was documented.

Pathologic Response—Assessment of pathologic response was performed at the treating site and reviewed at CPL-VCU. pCR is defined as an absence of viable invasive tumor at histopathologic examination of a posttherapy breast surgical specimen. Residual ductal carcinoma in situ in the absence of viable invasive cancer was considered a pCR. Dichotomous response assessment was performed, with a result of either pCR or no-pCR.

Residual Cancer Burden Categories—A secondary measure assessed the RCB at CPL-VCU. The RCB was calculated as an index combining pathology measurements as described previously (18). There were 4 RCB categories: RCB 0 (pCR), RCB 1 (minimal residual disease), RCB 2 (moderate residual disease), and RCB 3 (extensive residual disease or chemoresistant).

LN Status Analysis—The participating sites' pathology reports were reviewed for LN status. In the case of a positive LN, a section of the LN was requested if size was unavailable from the report. In positive cases when a section was unavailable, if the original pathology report indicated macrometastasis, the size was assumed greater than 2 mm.

Ki-67 Analysis—An index of cellular proliferation was determined on pre- and posttreatment paraffin-embedded specimens (3- to 5-μm sections), by immunohistochemistry using monoclonal mouse antihuman Ki-67 antigen (clone MIB-1; DAKO Denmark A/S). A Ki-67 score was defined as the percentage of total number of tumor cells with nuclear staining over the total number of tumor cells in 10 high-power fields (at 400×, Eclipse 80i light microscope [Nikon]) (20). The Ki-67 labeling index was also calculated as the number of Ki-67–positive tumor cells per one thousand tumor cells.

Adverse Effect Assessment

An adverse event evaluation form was completed after all imaging time points. All adverse events were recorded within a 24-h period.

Statistical Analysis

Data were analyzed using SAS (version 9.4; SAS Institute) and R software (version 3.1.0; R project, www.r-project.org). The study was designed to accrue 54 patients (including 10% dropout) to detect a difference of 0.25 in AUC (area under the receiver-operating-characteristic [ROC] curve) between the null hypothesis (AUC, 0.50, i.e., by chance) and the alternative hypothesis (true AUC 0.75) with the significance level 0.05 and power 0.80. The pCR rate was assumed to be 0.25 in the sample size calculation. The percentage change was defined as (SUV at FLT1 – SUV at FLT2)/SUV at FLT1 × 100 (% $SUV_{max\_FLT1-FLT2}$). The pCR was based on the pathology results as described above. The empiric AUC was calculated, and the 90% confidence interval (CI) was constructed from 2,000 bootstrapping. The optimal cutoff on the ROC curve was estimated using the Youden index method (21). The corresponding sensitivity and specificity were then calculated with the optimal cutoff for using the percentage change to detect pCR. The Delong method was used to test if the observed AUC was significantly greater than 0.5 with the 1-sided *P* value (22). We also tested if SUV reduction in the pCR group was significantly larger than that in the no-pCR group using the Wilcoxon method with 1-sided *P* value. A key secondary objective was to evaluate the correlation between SUV and Ki-67 labeling index at the baseline PET and at the PET after the treatment. This correlation was quantified by the Spearman correlation coefficient (*r*) using the Cohen and Cohen method (23). For the LN evaluation, a 3-category grouping was first implemented (i.e., 0 positive nodes, 1–3 positive nodes, and >3 positive nodes), and then Kruskal–Wallis 1-way ANOVA was conducted to compare SUV distributions among groups with 2-sided *P* values. For RCB

evaluation, the 4 categories were binned into 2 groups (RCB 0 and 1 vs. RCB 2 and 3) (18), and the comparison was conducted by Wilcoxon 2-sample test with 2-sided exact *P* value reported. The logistic regression was also fitted to quantify the association of the dichotomized RCB with % $SUV_{max\_FLT1-FLT2}$ or % $SUV_{max\_FLT1-FLT3}$.

RESULTS

Ninety patients were registered by 17 participating institutions (Supplemental Table 1; supplemental materials are available at http://jnm.snmjournals.org), between November 2009 and August 2012. All institutions had Institutional Review Board approval of the protocol, and all patients signed the informed consent form. Fifty-one of 90 patients were eligible for the primary objective analysis and completed both FLT1 and FLT2 scans within the study timeline. The remaining 39 patients did not fulfill the primary aim eligibility criteria for various reasons (Supplemental Tables 2 and 3). Up to 73 patients met the eligibility criteria for the secondary objective analyses correlating ^{18}F-FLT uptake to the Ki-67, including 72 patients undergoing FLT1 and 43 undergoing FLT3. The patient characteristics are displayed in Table 1. All patients tolerated the ^{18}F-FLT PET/CT protocol, and none suffered significant study-related adverse effects.

Inherent to the protocol design, chemotherapy protocols and timing varied significantly among participants (Supplemental Table 4). There was some variability in uptake times, related to optional dynamic scans performed at several sites (not included in this analysis). However, uptake times from the same patient in serial scans were similar (Supplemental Table 5). Treatment for more than 60% of the patients included a combination of doxorubicin with cyclophosphamide, followed or preceded by a taxane.

Primary Objectives

^{18}F-FLT PET/CT Imaging and pCR—Of 51 patients eligible for primary objective analysis, 43 completed all FLT1, FLT2, and FLT3 imaging studies, and 8 completed only FLT1 and FLT2 studies. All evaluable patients had measurable disease in the breast (>2.0 cm, median, 4.0 cm; range, 2.0–13.0 cm). In large tumors, regions of imaging-based necrosis were excluded from the analysis. A pCR was achieved in 9 (18%) patients; of the remaining 42 (82%) patients who had a no-pCR, 31 (73%) had partial and 11 (26%) had no pathologic response. The median interval between FLT1 and initiation of chemotherapy was 3 d (range, 1–38 d), median interval between first chemotherapy and FLT2 was 7 d (range, 3–17 d), and in all cases FLT2 was before the second NAC cycle; median interval between FLT3 and surgery was 8 d (range, 1–70 d).

% $SUV_{max\_FLT1-FLT2}$ by pCR—Examples of serial ^{18}F-FLT PET/CT studies are shown in Figures 1 and 2. The FLT1 SUV_{max} was not different between pCR and no-pCR groups (mean ± SD, 6.1 ± 3.2 vs. 5.6 ± 3.0; difference, −0.5 ± 3.0; 95% CI, −2.7–1.7, *P* = 0.62) (Table 2; Supplemental Tables 6 and 7). The % $SUV_{max\_FLT1-FLT2}$ changes are presented in Table 3. There was a marginal difference in % $SUV_{max\_FLT1-FLT2}$ between pCR and no-pCR patients (Wilcoxon, 1-sided *P* = 0.050). The corresponding value for % $SUV_{peak\_FLT1-FLT2}$ and % $SUV_{mean\_FLT1-FLT2}$ were similar (*P* = 0.056, 0.033, respectively).

ROC Analysis of % SUV$_{max\_FLT1-FLT2}$ in Predicting pCR—The AUC for % SUV$_{max\_FLT1-FLT2}$ was 0.68 (90% CI, 0.50–0.83, Delong 1-sided $P = 0.046$) (Fig. 3), which is marginally significant from the null hypothesis of AUC = 0.50. The AUC for % SUV$_{peak\_FLT1-FLT2}$ was 0.67 (90% CI, 0.50–0.82, Delong 1-sided $P = 0.044$). The AUC for % SUV$_{mean\_FLT1-FLT2}$ was 0.70 (90% CI, 0.54–0.84, Delong 1-sided $P = 0.016$). The optimal cutoff of % SUV$_{max\_FLT1-FLT2}$ was 51% from the Youden index, and the corresponding sensitivity and specificity were 0.56 (95% CI, 0.21–0.86) and 0.79 (95% CI, 0.63–0.90), respectively.

Secondary Objectives

% SUV$_{max\_FLT1-FLT3}$ by pCR—Of 43 patients who underwent both FLT1 and FLT3 scans, the mean reduction in SUV$_{max}$ (% SUV$_{max\_FLT1-FLT3}$) was 67% (range, –4%–96%) (Table 3). There was a significant difference in % SUV$_{max\_FLT1-FLT3}$ between 8 pCR and 35 no-pCR patients (Wilcoxon, 1-sided $P = 0.0013$). The corresponding values for % SUV$_{mean\_FLT1-FLT3}$ and % SUV$_{peak\_FLT1-FLT3}$ were also similar (not shown). The AUC for % SUV$_{max\_FLT1-FLT3}$ in the prediction of pCR was 0.83 (90% CI, 0.72–0.94, Delong 1-sided $P < 0.001$) (Fig. 4). The AUC for % SUV$_{peak\_FLT1-FLT3}$ was 0.82 (90% CI, 0.69–0.92, Delong 1-sided $P < 0.001$), and AUC for % SUV$_{mean\_FLT1-FLT3}$ was 0.80 (90% CI, 0.68–0.92, Delong 1-sided $P < 0.001$).

Correlation Between ^{18}F-FLT SUV$_{max}$ and Ki-67 Expression—Suitable histopathology was available in 72 of the 90 recruited patients. There was a weak correlation between FLT1 SUV$_{max}$ and Ki-67 ($r = 0.35$; 95% CI, 0.13–0.54; $P = 0.002$, Fig. 5).

There were 43 patients who had suitable post-NAC tissue samples for correlation between surgical specimens and FLT3 SUVs. There was an improved correlation between FLT3 and Ki-67 ($r = 0.68$; 95% CI, 0.47–0.81; $P < 0.0001$, Fig. 6), compared with that of FLT1 and Ki-67 ($P = 0.020$ for the difference in correlations). The correlation between % SUV$_{max\_FLT1-FLT3}$ and % Ki-67$_{FLT1-FLT3}$ was 0.57 (95% CI, 0.35–0.75; $P < 0.0001$) from the analysis of 42 patients who had Ki-67 expressions at both FLT1 and FLT3 time points.

LN Evaluation—Data on 38 patients were available for histopathologic LN evaluation after NAC: 14 with negative nodes, 15 with 1–3 LN metastases, and 9 with more than 3 LN metastases. The mean SUV$_{max}$ was not different among the 3 groups—FLT1, FLT2, and FLT3—at any time point (Supplemental Table 8). In patients with negative nodes, mean ^{18}F-FLT SUV$_{max}$ at FLT1 and FLT3 were 4.4 ± 3.0 and 0.8 ± 0.4, respectively, compared with 6.6 ± 3.6 and 1.2 ± 0.7 for those with 1–3 positive LNs after NAC (or with 7.3 ± 5.0 and 2.5 ± 2.2 for those with >3 positive nodes after NAC).

% SUV$_{max\_FLT1-FLT2}$ and LN Status at Surgery—The % SUV$_{max\_FLT1-FLT2}$ and % SUV$_{max\_FLT1-FLT3}$ were not associated with the LN status; the mean % SUV$_{max\_FLT1-FLT2}$ and % SUV$_{max\_FLT1-FLT3}$ were not different among negative (0 positive LNs), 1–3 positive, and more than 3 positive groups (Supplemental Table 9).

^{18}F-FLT PET/CT and Primary Tumor RCB—Suitable histopathology was available in 35 patients for RCB evaluation: 14 patients with RCB 0 or 1 and 21 patients with RCB 2 or 3. The SUV_{max} measurements at FLT1 and FLT2 were not different between these 2 groups (P = not significant) whereas there was a difference in SUV_{max} at FLT3 (P = 0.010) (Supplemental Table 10). The % $SUV_{max\_FLT1-FLT2}$ was not associated with RCB when RCB was dichotomized (P = not significant) whereas % $SUV_{max\_FLT1-FLT3}$ was ($P <$ 0.001); the mean values were different between the 2 groups at FLT3 (Supplemental Table 11). The magnitude of % $SUV_{max\_FLT1-FLT3}$ tended to be associated with lower RCB when RCB was evaluated as a dichotomized variable (RCB 0–1 vs. RCB 2–3 (13)) (odds ratio for % $SUV_{max\_FLT1-FLT3}$, 0.86; 95% CI, 0.76–0.97, P = 0.013).

Adverse Effects—There were no severe or life-threatening events. In total, there were 20 adverse events. Only 2 mild adverse events were considered to be possibly related to ^{18}F-FLT injection; both were patient complaints of facial warmth during scanning.

DISCUSSION

Changes of proliferative status of breast cancer measured by tissue assay early after chemotherapy or endocrine therapy are predictive of outcome (24). Furthermore, ^{18}F-FLT PET, as a surrogate of cell proliferation, was shown to detect therapy-induced proliferative changes as early as 1 wk after chemotherapy (11,13). In our study testing ^{18}F-FLT PET as a predictor of tumor response to NAC after a single treatment dose, we found a marginal predictive value of % $SUV_{max\_FLT1-FLT2}$ for pCR, with AUCs in the range of 0.66–0.70 for different measures of ^{18}F-FLT uptake. The % SUVs of FLT1 to FLT2 or FLT1 to FLT3 were not associated with the axillary LN status at surgery. We also found that posttherapy ^{18}F-FLT uptake had a significant correlation with the Ki-67 proliferative index in post-therapy surgical specimens, further supporting ^{18}F-FLT as a marker of tumor proliferation and therapeutic response. Additionally, the change between pretherapy and posttherapy ^{18}F-FLT PET (FLT1–FLT3) was a strong indicator of pCR, with AUCs of 0.80–0.83. However, whereas our results suggest an ability of early serial ^{18}F-FLT PET/CT to predict therapeutic response, the accuracy of this predictive value was modest.

There has been variability in the published studies for ^{18}F-FLT PET/CT as an early indicator of response. Small, single-center preliminary studies indicated good predictive value for response (11–14), whereas others did not (12,15–17). Our multicenter study suggested some utility for ^{18}F-FLT as an early predictor of response, but preliminary reports of other multicenter trials did not find a predictive value for ^{18}F-FLT (25). The difference between our study and the previous others likely lies with variations in endpoints (clinical vs. pathologic response), image acquisition and analysis methods, patient populations, and therapy regimens. None of the prior studies investigated the potential of ^{18}F-FLT PET imaging for predicting pCR to NAC but rather investigated overall clinical response (11), changes in tumor size and in tumor markers in patients with all stages including distant metastasis (13). Our study had the advantage of having a slightly larger patient population, rigorous central system qualification, and image and pathologic analyses. Although there was some variability in ^{18}F-FLT uptake time in our study due to the optional dynamic imaging protocol, uptake times for each patient across longitudinal PET scans were

reasonably consistent. The published results of multiple prospective studies indicated that early ^{18}F-FDG PET can reasonably predict pathologic response to NAC in breast cancer (26–29). Our results on ^{18}F-FLT PET were comparable with the prior published data by showing that NAC resulted in a significant SUV_{max} reduction (mean , 39%; cutoff, 51%) despite a marginal significance between pCR and no-pCR groups. However, the relatively small number of patients with a pCR as well as the varying definitions of the pCR across studies should be taken into consideration when comparing our results with others.

The main limitation of our study was that it did not control treatment types, and there was a considerable variation in chemo-therapeutic regimens—both type and frequency of treatments—across participating centers, resulting in variable definitions of 1 treatment cycle. This likely contributes to variability in ^{18}F-FLT results between patients and limits the overall performance of ^{18}F-FLT PET as an early indicator of response in our study. Variability in scan timing and timing relative to treatment may also have contributed to variable performance. In our cohort, only 18% of patients had a pCR, a result that is consistent with other trials in locally advanced breast cancer, using standard anthracycline–taxane combination chemotherapy in patients with heterogeneous tumor subtypes (30–32). It is also important to realize the unbalanced number of patients between the pCR and no-pCR groups (9 vs. 42). The limited number of patients with a pCR may have limited the ability to identify differences between high and low % SUV between baseline and after 1 cycle of therapy. Further studies comparing changes in ^{18}F- FLT to longer-term survival endpoints might yield further insights but was beyond the scope of this study. Similarly, a recent study by Woolf et al. (15) reported that neither the baseline value nor the change in SUV_{max} after 1 cycle of NAC predicted treatment response, although most patients had a sizeable SUV_{max} reduction. Likewise, in our study, the mean decline in $SUV_{max\_FLT1-FLT2}$ was 39%. Some data using tissue markers of proliferation suggest better predictive value in more aggressive tumor subtypes (e.g., human epidermal growth factor receptor type 2–positive, basal, or triple-negative cancers) and that these different tumor subtypes may have different responsiveness to cytoxic chemotherapy regimens (33,34,). ^{18}F-FDG PET was shown to be most predictive in high-risk breast cancer phenotypes (4,5). Our data were not conducive to perform subgroup analysis with respect to various risk groups—that is, triple-negative, human epidermal growth factor receptor type 2–positive, because it was not powered for analyzing tumor subtypes. This analysis remains to be further pursued in future studies.

As a secondary objective, correlation with Ki-67 revealed only a weak correlation between SUV_{max} at FLT1 and Ki-67 expression from pretherapy biopsy specimens, but a better correlation was found between FLT3 SUV_{max} and Ki-67 in posttherapy surgical specimens. Although prior studies found a correlation between ^{18}F-FLT uptake and Ki-67 expression (10,13,15), these results varied depending on both sample acquisition and postacquisition treatment of tissues, possibly affecting direct comparisons. A recent breast cancer study demonstrated a significant difference between pretherapy core biopsy and surgical sample Ki-67 values ($P < 0.0001$) in paired samples from untreated patients (35). Importantly, the difference represented an average difference in proliferation, with the core biopsies demonstrating a higher proliferation index than the surgical samples. Another factor potentially contributing to a variable pretherapy relationship between ^{18}F-FLT uptake and

Ki-67 is the range of included tumor subtypes; some preclinical studies suggested that ^{18}F-FLT uptake and its correlation with Ki-67 may vary across tumor types (36). In our study, the weaker correlation in pretherapy biopsy samples compared with surgical specimens may also be related to intratumor spatial heterogeneity of cell proliferation (37). A meta-analysis by Chalkidou et al. showed that the ^{18}F-FLT uptake and Ki-67 correlation was significant and independent of cancer type (38). They also reported that the whole surgical specimen provided a significant correlation, whereas biopsy samples did not. This finding is in line with our results. The agreement between posttherapy ^{18}F-FLT and Ki-67 supports the utility of ^{18}F-FLT as a response marker, as does a more robust ability to discern pCR on the basis of differences between the pre- and posttherapy ^{18}F-FLT uptake (AUC = 0.80–0.83 for different SUV measures).

Some studies suggest that kinetic analysis of ^{18}F-FLT uptake in breast cancer reportedly correlated better with Ki-67 than SUVs for distinguishing responders from nonresponders early during chemotherapy (8,39). We collected kinetic data in a select group of patients, but these results will be reported separately.

Residual disease is a continuous variable consisting of a range of tissue responses from complete response to refractory disease. The RCB index was proposed as a determinant of the extent of residual disease in the surgical specimens after NAC (18). The % $SUV_{max\_FLT1-FLT3}$ predicted RCB when RCB was evaluated as a continuous or dichotomized variable. The absolute SUV_{max} measurements at FLT1 and FLT2 were not different between the RCB groups; however, there was a significant difference in posttherapy FLT SUV_{max} (FLT3) for RCB 0–1 versus RCB 2 or greater.

CONCLUSION

^{18}F-FLT PET/CT imaging of breast cancer after 1 cycle of NAC was marginally predictive of pCR despite highly variable chemotherapy regimens. Posttherapy NAC ^{18}F-FLT uptake correlated with assay of Ki-67 on postsurgical tissue and with pCR. These early results, though not sufficient to support widespread use of ^{18}F-FLT as an early response indicator for breast cancer, indicate the potential efficacy of ^{18}F-FLT PET/CT as an indicator of early therapeutic response of breast cancer to NAC and support future studies in a more uniformly treated patient population.

Supplementary Material

Refer to Web version on PubMed Central for supplementary material.

Acknowledgments

References

1. Chia S, Swain SM, Byrd DR, et al. Locally advanced and inflammatory breast cancer. J Clin Oncol. 2008; 26:786–790. [PubMed: 18258987]

2. Berruti A, Amoroso V, Gallo F, et al. Pathologic complete response as a potential surrogate for the clinical outcome in patients with breast cancer after neoadjuvant therapy: a meta-regression of 29 randomized prospective studies. J Clin Oncol. 2014; 32:3883–3891. [PubMed: 25349292]

3. Cortazar P, Zhang L, Untch M, et al. Pathological complete response and long-term clinical benefit in breast cancer: the CTNeoBC pooled analysis. Lancet. 2014; 384:164–172. [PubMed: 24529560]

4. Hatt M, Groheux D, Martineau A, et al. Comparison between ^{18}F-FDG PET image-derived indices for early prediction of response to neoadjuvant chemotherapy in breast cancer. J Nucl Med. 2013; 54:341–349. [PubMed: 23327900]

5. Groheux D, Hindié E, Giacchetti S, et al. Early assessment with ^{18}F-fluorodeoxyglucose positron emission tomography/computed tomography can help predict the outcome of neoadjuvant chemotherapy in triple negative breast cancer. Eur J Cancer. 2014; 50:1864–1871. [PubMed: 24841218]

6. Shields AF, Grierson JR, Dohmen BM, et al. Imaging proliferation in vivo with [F-18]FLT and positron emission tomography. Nat Med. 1998; 4:1334–1336. [PubMed: 9809561]

7. Bading JR, Shields AF. Imaging of cell proliferation: status and prospects. J Nucl Med. 2008; 49(suppl 2):64S–80S. [PubMed: 18523066]

8. Chang ZF, Huang DY, Hsue NC. Differential phosphorylation of human thymidine kinase in proliferating and M phase arrested human cells. J Biol Chem. 1994; 269:21249–21254. [PubMed: 8063748]

9. Munch-Petersen B, Cloos L, Jensen HK, Tyrsted G. Human thymidine kinase. I. Regulation in normal and malignant cells. Adv Enzyme Regul. 1995; 35:69–89. [PubMed: 7572355]

10. Kenny LM, Vigushin DM, Al-Nahhas A, et al. Quantification of cellular proliferation in tumor and normal tissues of patients with breast cancer by [^{18}F] fluorothymidine-positron emission tomography imaging: evaluation of analytical methods. Cancer Res. 2005; 65:10104–10112. [PubMed: 16267037]

11. Kenny L, Coombes RC, Vigushin DM, et al. Imaging early changes in proliferation at 1 week post chemotherapy: a pilot study in breast cancer patients with 3-deoxy-3-[^{18}F]fluorothymidine positron emission tomography. Eur J Nucl Med Mol Imaging. 2007; 34:1339–1347. [PubMed: 17333178]

12. Contractor KB, Kenny LM, Stebbing J, et al. ^{18}F]-3′deoxy-3′-fluorothymidine positron emission tomography and breast cancer response to docetaxel. Clin Cancer Res. 2011; 17:7664–7672. [PubMed: 22028493]

13. Pio BS, Park CK, Pietras R, et al. Usefulness of 3′-[F-18]fluoro-3-deoxythymidine with positron emission tomography in predicting breast cancer response to therapy. Mol Imaging Biol. 2006; 8:36–42. [PubMed: 16362149]

14. Marti-Climent JM, Dominguez-Prado I, Garcia-Velloso MJ, et al. [^{18}F]fluorothymidine-positron emission tomography in patients with locally advanced breast cancer under bevacizumab treatment: usefulness of different quantitative methods of tumor proliferation. Rev Esp Med Nucl Imagen Mol. 2014; 33:280–285. [PubMed: 25066253]

15. Woolf DK, Beresford M, Li SP, et al. Evaluation of FLT-PET-CT as an imaging biomarker of proliferation in primary breast cancer. Br J Cancer. 2014; 110:2847–2854. [PubMed: 24832174]

16. Contractor K, Aboagye EO, Jacob J, et al. Monitoring early response to taxane therapy in advanced breast cancer with circulating tumor cells and [^{18}F] 3′-deoxy-3′-fluorothymidine PET: a pilot study. Biomark Med. 2012; 6:231–233. [PubMed: 22448798]

17. Couturier O, Rousseau C, Pierga J-Y, et al. 3′-deoxy-3′-[18F]fluorothymidine (18F-FLT) positron emission tomography (PET): an accurate and effective tool for assessing tumor response in breast cancer. Cancer Res. 2013; 73(24 suppl):P4-01–05.

18. Symmans WF, Peintinger F, Hatzis C, et al. Measurement of residual breast cancer burden to predict survival after neoadjuvant chemotherapy. J Clin Oncol. 2007; 25:4414–4422. [PubMed: 17785706]

19. Scheuermann JS, Saffer JR, Karp JS, Levering AM, Siegel BA. Qualification of PET scanners for use in multicenter cancer clinical trials: the American College of Radiology Imaging Network experience. J Nucl Med. 2009; 50:1187–1193. [PubMed: 19525463]

20. Dowsett M, Nielsen TO, A'Hern R, et al. Assessment of Ki67 in breast cancer: recommendations from the International Ki67 in Breast Cancer working group. J Natl Cancer Inst. 2011; 103:1656–1664. [PubMed: 21960707]

21. Youden WJ. Index for rating diagnostic tests. Cancer. 1950; 3:32–35. [PubMed: 15405679]

22. DeLong ER, DeLong DM, Clarke-Pearson DL. Comparing the areas under two or more correlated receiver operating characteristic curves: a nonparametric approach. Biometrics. 1988; 44:837–845. [PubMed: 3203132]

23. Cohen, J.; Cohen, P. Applied Multiple Regression/Correlation Analysis for the Behavioral Science. 2. Hillsdale, NJ: Lawrence Erlbaum Associates; 1983.

24. Ellis MJ, Suman VJ, Hoog J, et al. Randomized phase II neoadjuvant comparison between letrozole, anastrozole, and exemestane for post-menopausal women with estrogen receptor-rich stage2 to 3 breast cancer: clinical and biomarker outcomes and predictive value of the baseline PAM50-based intrinsic subtype ACOSOG Z1031. J Clin Oncol. 2011; 29:2342–2349. [PubMed: 21555689]

25. Schmidt, EV.; Blackman, S.; Iannone, R., et al. Limits of [^{18}F]-FLT PET as a clinical biomarker of proliferation in breast cancer. Poster Session 4. Detection and Diagnosis: Molecular, Functional, and Novel Imaging. Poster presented at SABCS; December 13, 2013; San Antonio, Texas.

26. Rousseau C, Devillers A, Sagan C, et al. Monitoring of early response to neo-adjuvant chemotherapy in stage II and III breast cancer by [^{18}F]fluorodeoxyglucose positron emission tomography. J Clin Oncol. 2006; 24:5366–5372. [PubMed: 17088570]

27. Berriolo-Riedinger A, Touzery C, Riedinger JM, et al. [^{18}F]FDG-PET predicts complete pathological response of breast cancer to neoadjuvant chemotherapy. Eur J Nucl Med Mol Imaging. 2007; 34:1915–1924. [PubMed: 17579854]

28. Schwarz-Dose J, Untch M, Tiling R, et al. Monitoring primary systemic therapy of large and locally advanced breast cancer by using sequential positron emission tomography imaging with [^{18}F]fluorodeoxyglucose. J Clin Oncol. 2009; 27:535–541. [PubMed: 19075273]

29. Kolesnikov-Gauthier H, Vanlemmens L, Baranzelli MC, et al. Predictive value of neoadjuvant chemotherapy failure in breast cancer using FDG-PET after the first course. Breast Cancer Res Treat. 2012; 131:517–525. [PubMed: 22037787]

30. Frasci G, D'Aiuto G, Comella P, et al. Weekly cisplatin, epirubicin, and paclitaxel with granulocyte colony–stimulating factor support vs triweekly epirubicin and paclitaxel in locally advanced breast cancer: final analysis of a SICOG phase III study. Br J Cancer. 2006; 95:1005–1012. [PubMed: 17047649]

31. Villman K, Ohd JF, Lidbrink E, et al. A phase II study of epirubicin, cisplatin and capecitabine as neoadjuvant chemotherapy in locally advanced or inflammatory breast cancer. Eur J Cancer. 2007; 43:1153–1160. [PubMed: 17398088]

32. Ellis GK, Barlow WE, Gralow JR, et al. Phase III comparison of standard doxorubicin and cyclophosphamide versus weekly doxorubicin and daily oral cyclophosphamide plus granulocyte colony-stimulating factor as neoadjuvant therapy for inflammatory and locally advanced breast cancer: SWOG 0012. J Clin Oncol. 2011; 29:1014–1021. [PubMed: 21220618]

33. Carlomagno C, Perrone F, Gallo C, et al. c-erbB2overexpression decreases the benefit of adjuvant tamoxifen in early-stage breast cancer without axillary lymph node metastases. J Clin Oncol. 1996; 14:2702–2708. [PubMed: 8874330]

34. Pritchard KI, Shepherd LE, O'Malley FP, et al. HER2 and responsiveness of breast cancer to adjuvant chemotherapy. N Engl J Med. 2006; 354:2103–2111. [PubMed: 16707747]

35. Romero Q, Bendahl PO, Klintman M, et al. Ki67 proliferation in core biopsies versus surgical samples: a model for neo-adjuvant breast cancer studies. BMC Cancer. 2011; 11:341. [PubMed: 21819622]

36. Zhang CC, Yan Z, Li W, Kuszpit K, et al. Clin Cancer Res. 2012; 18:1303–1312. [PubMed: 22170262]

37. Willaime JM, Turkheimer FE, Kenny LM, Aboagye EO. Quantification of intra-tumour cell proliferation heterogeneity using imaging descriptors of ^{18}F fluorothymidine-positron emission tomography. Phys Med Biol. 2013; 58:187–203. [PubMed: 23257054]

38. Chalkidou A, Landau DB, Odell EW, et al. Correlation between Ki-67 immunohistochemistry and ^{18}F-fluorothymidine uptake in patients with cancer: a systematic review and meta-analysis. Eur J Cancer. 2012; 48:3499–3513. [PubMed: 22658807]

39. Gray KR, Contractor KB, Kenny LM, et al. Kinetic filtering of [^{18}F] fluorothymidine in positron emission tomography studies. Phys Med Biol. 2010; 55:695–709. [PubMed: 20071760]
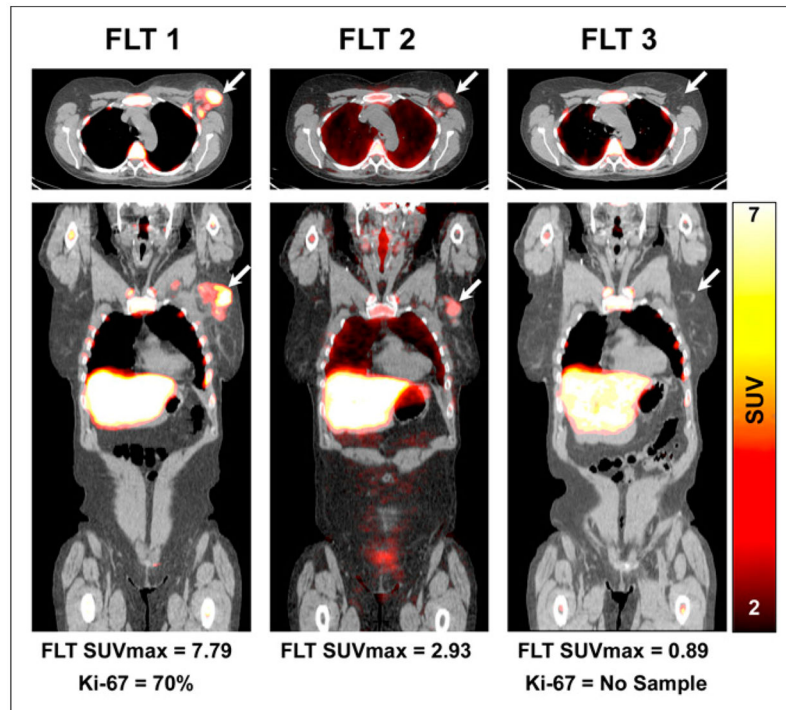
FIGURE 1.

^{18}F-FLT PET/CT axial (upper) and coronal (lower) images demonstrate increased ^{18}F-FLT uptake in an upper outer quarter breast tumor and axillary LN, before therapy (left) with substantial reduction in primary breast tumor ^{18}F-FLT uptake after 1 cycle of NAC (middle) and resolution of ^{18}F-FLT uptake after completion of NAC (right). Patient had pCR confirmed at surgery. Arrows refer to primary tumor site.
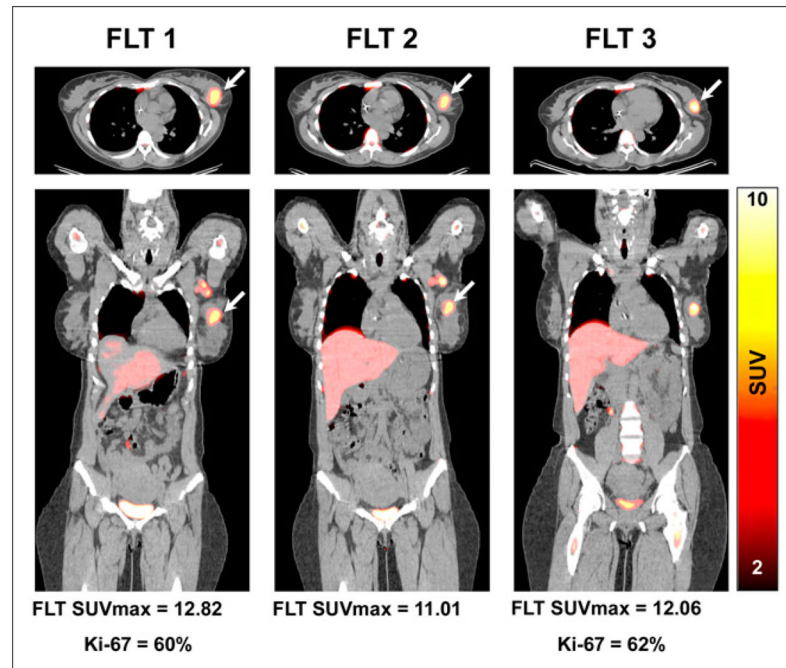
FIGURE 2.

^{18}F-FLT PET/CT axial (upper) and coronal (lower) images demonstrate increased ^{18}F-FLT uptake in upper outer quarter breast tumor before therapy (left) with minimal decline in uptake and after 1 cycle of NAC (middle) and significant residual uptake after completion of NAC (right). At surgery, significant residual viable tumor was confirmed (i.e., no-pCR) with high Ki-67 index (62%). Arrows refer to primary tumor site.
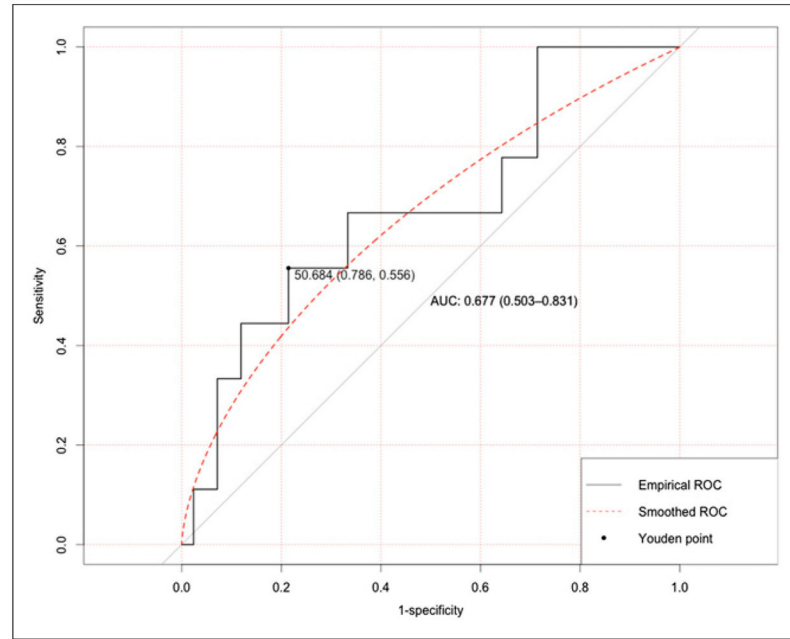
FIGURE 3.
ROC curve of using % $SUV_{max\_FLT1-FLT2}$ to predict pCR. Optimal cut point with corresponding specificity and sensitivity was identified through Youdan index.
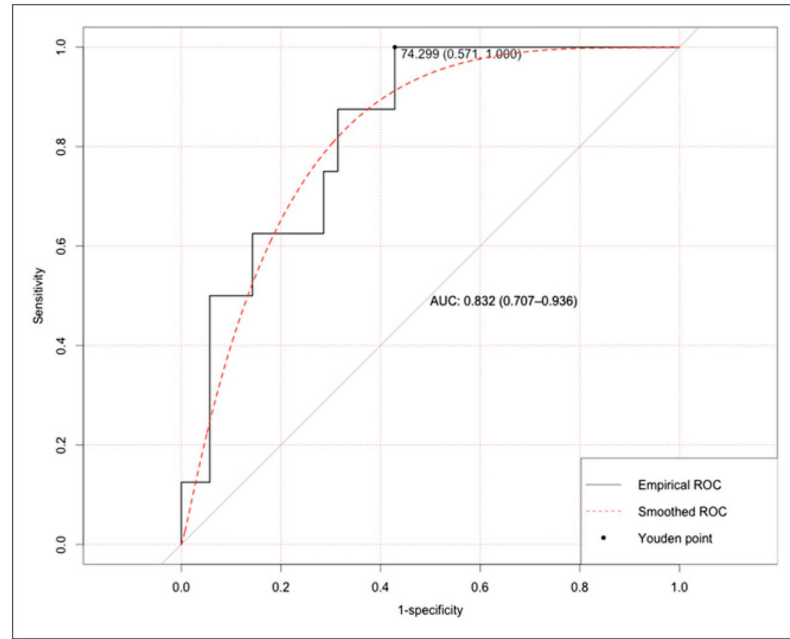
FIGURE 4.
ROC curve of using % $SUV_{max\_FLT1\text{-}FLT3}$ to predict pCR. Optimal cut point with corresponding specificity and sensitivity was identified through Youdan index.
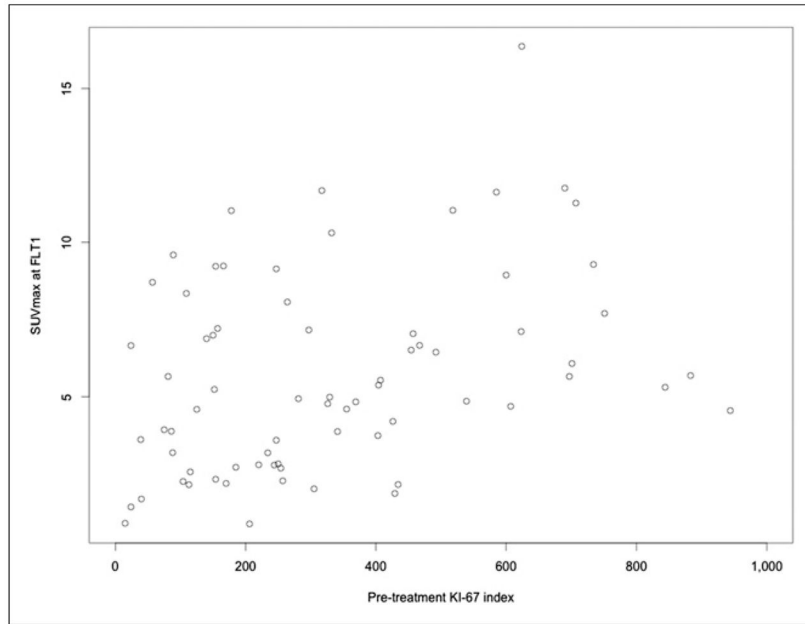
FIGURE 5.
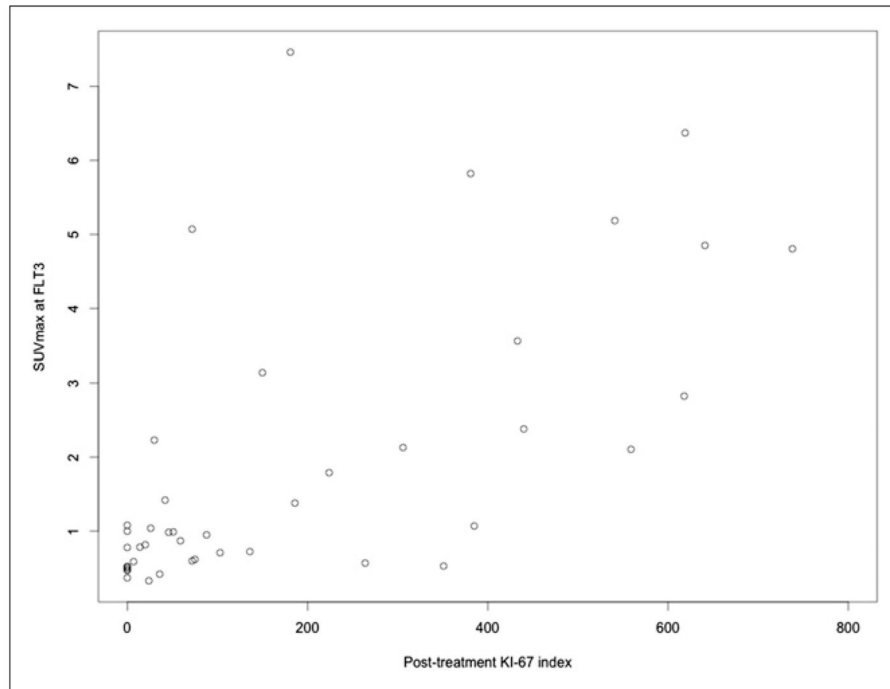Scatterplot for Ki-67 on biopsy specimens versus SUV$_{max}$ at FLT1.

FIGURE 6.
Scatterplot for Ki-67 on surgical specimens versus SUV$_{max}$ at FLT3.

TABLE 1

Patient Demographics

Demographic	Variable	All registered patients	Primary aim analysis ($n = 51$)	Ki-67 analysis ($n = 73$)
Mean age ± SD (y)		51.3 ± 10.9	52.5 ± 10.6	51.5 ± 10.2
Ethnicity	Hispanic or Latino	9 (10%)	3 (5.9%)	6 (8.2%)
	Not Hispanic or Latino	75 (83.3%)	43 (84.3%)	62 (84.9%)
	American Indian, Alaska Native, Asian	3 (3.3%)	2 (4%)	3 (4.1%)
	Black or African American	25 (27.8%)	12 (23.5%)	19 (26%)
	White	51 (56.7%)	32 (62.7%)	43 (58.9%)
Mean tumor size ± SD (cm)		4.4 ± 2.5	4.6 ± 2.5	4.4 ± 2.4
Menopausal status	Premenopausal	42 (46.7%)	22 (43.1%)	33 (45.2%)
	Postmenopausal	47 (52.2%)	29 (56.9%)	39 (53.4%)
Initial diagnosis	Invasive breast cancer NOS	2 (2.2%)	2 (3.9%)	2 (2.7%)
	Invasive ductal	77 (85.5%)	43 (84.4%)	63 (86.3%)
	Invasive lobular + mixed invasive & lobular	10 (11.1%)	6 (11.8%)	8 (11%)
Estrogen receptor status	Positive	49 (54.4%)	29 (56.9%)	43 (58.9%)
	Negative	40 (44.4%)	22 (43.1%)	30 (41.1%)
Progesterone receptor status	Positive	38 (42.2%)	20 (39.2%)	35 (47.9%)
	Negative	51 (56.7%)	31 (60.8%)	38 (52.1%)
HER2 status	Positive	32 (35.6%)	15 (29.4%)	22 (30.1%)
	Negative	54 (60%)	34 (66.7%)	48 (65.8%)
Receptor status	Triple negative	22 (24.4%)	13 (25.5%)	19 (26%)
	Other	64 (71.1%)	36 (70.6%)	51 (69.9%)
T stage	TX	3 (3.3%)	3 (5.9%)	3 (4.1%)
	T1	1 (1.1%)	NA	NA
	T2	42 (46.7%)	23 (45.1%)	35 (47.9%)
	T3	31 (34.4%)	19 (37.3%)	25 (34.2%)
	T4	12 (13.3%)	6 (11.7%)	10 (13.7%)
Pathologic N stage	pNX	3 (3.3%)	3 (5.9%)	3 (4.1%)
	pN0	26 (28.9%)	13 (25.5%)	23 (31.5%)
	pN1	45 (50.0%)	27 (53%)	35 (48.0%)
	pN2	10 (11.1%)	5 (9.8%)	8 (11%)
	pN3	5 (4.4%)	3 (5.9%)	4 (5.5%)
Stage	IIA	19 (21.1%)	10 (19.6%)	16 (21.9%)
	IIB	32 (35.6%)	18 (35.3%)	26 (35.6%)
	IIIA	22 (24.4%)	14 (27.5%)	18 (24.7%)
	IIIB	9 (10%)	5 (9.8%)	8 (11%)
	IIIC	4 (4.4%)	3 (5.9%)	4 (5.5%)

Demographic	Variable	All registered patients	Primary aim analysis ($n = 51$)	Ki-67 analysis ($n = 73$)
	IV	2 (2.2%)	NA	NA
Grade at diagnosis	1	2 (2.2%)	1 (2%)	2 (2.7%)
	2	19 (21.1%)	12 (23.5%)	17 (23.3%)
	3	44 (48.9%)	27 (52.9%)	33 (45.2%)

Percentages not adding up to 100% are due to missing data; tumor size was determined using baseline imaging.

NOS = not otherwise specified; HER2 = human epidermal growth factor receptor type 2; NA = not applicable.

TABLE 2

Distributions of SUV_{max} and Ki-67 Across Different Time Points

Time point	Aim	Parameter tested	pCR status	No. of evaluable participants	Range	Mean	SD	P^*
Baseline (FLT1)	Primary aim	SUV_{max}	All data	51	0.87–11.76	5.65	2.97	0.62
			pCR	9	1.86–11.76	6.09	3.17	
			no-pCR	42	0.87–11.68	5.55	2.95	
After 1 cycle of NAC (FLT2)	Primary aim	SUV_{max}	All data	51	0.44–8.29	3.21	1.84	0.35
			pCR	9	0.92–8.29	3.00	2.54	
			No-pCR	42	0.44–6.43	3.25	1.69	
After completion of NAC (FLT3)	FLT3 secondary aim	SUV_{max}	All data	43	0.33–7.46	1.74	1.81	0.0047
			pCR	8	0.37–1.08	0.62	0.27	
			No-pCR	35	0.33–7.46	2.00	1.92	
	Ki-67 secondary aim	Ki-67	All data	43	0–738	184.14	220.16	<0.001
			pCR	8	0–0	0.00	0.00	
			No-pCR	35	0–738	226.23	223.77	

*2-sided exact P value from Wilcoxon 2-sample test.

TABLE 3

Distributions of SUV Differences Between Time Points and by Pathologic Response Status

Difference	pCR status	no. of evaluable patients	Range	Mean (SD)	P^*
%SUV$_{max\_FLT1-FLT2}$	All data	51	−30.2–86.7	38.8 (26.1)	0.050
	pCR	9	24.7–84.3	52.7 (22.8)	
	No-pCR	42	−30.2–86.7	35.8 (26.0)	
%SUV$_{max\_FLT1-FLT3}$	All data	43	−4.04–96.1	66.9 (25.9)	0.0013
	pCR	8	74.5–96.1	86.9 (7.5)	
	No-pCR	35	−4.0–95.1	62.3 (26.5)	

*
1-sided exact *P* value from Wilcoxon 2-sample test.